

Article

Pipe Curtain Deformation and Surface Subsidence Caused via Excavation of Transverse Pilot Tunnel under Pipe Curtain Support

Qian Bai , Wen Zhao *, Yuan Sun and Xin Wang

School of Resources and Civil Engineering, Northeastern University, Shenyang 110819, China; baiqianneu@163.com (Q.B.); 13610830338@163.com (Y.S.); wangxin5010@163.com (X.W.)

* Correspondence: zhaowen@mail.neu.edu.cn

Abstract: Relying on the Shenyang Metro Line 4 Shifu Road station, the impact of the construction parameters of the transverse pilot tunnel on the surface subsidence and the pipe curtain deformation was first studied through numerical simulation, followed by the analysis of the impact of the excavation of the transverse pilot tunnel on the deformation characteristics of the pipe curtain through on-site monitoring. The results show the following: the excavation of the middle pilot tunnel is the key stage of the construction. The excavation sequence of H2 and H4 and H6 → H1 and H3 → H5 and H7 caused the least surface subsidence. Increasing the grouting width and improving the strength of the initial support can control the pipe curtain deformation very well, and it is reasonable to choose 1.5 m as the grouting width.

Keywords: subway station; pipe curtain method; transverse pilot tunnel; excavation; deformation response



Citation: Bai, Q.; Zhao, W.; Sun, Y.; Wang, X. Pipe Curtain Deformation and Surface Subsidence Caused via Excavation of Transverse Pilot Tunnel under Pipe Curtain Support. *Sustainability* **2023**, *15*, 11967. <https://doi.org/10.3390/su151511967>

Academic Editor: Jianjun Ma

Received: 30 June 2023

Revised: 30 July 2023

Accepted: 2 August 2023

Published: 3 August 2023



Copyright: © 2023 by the authors. Licensee MDPI, Basel, Switzerland. This article is an open access article distributed under the terms and conditions of the Creative Commons Attribution (CC BY) license (<https://creativecommons.org/licenses/by/4.0/>).

1. Introduction

Along with the continuous development of urban underground space in China, more and more subway stations have been built [1,2], and most subway stations are located in prosperous areas of cities [3–5]. The pile–beam–arch (PBA) method is a common method for constructing subway stations [6–8], but it is not suitable for subway station construction with high surface subsidence requirements owing to the large surface subsidence resulting from the buckle arch stage [9]. The pipe–roof structure can significantly reduce the surface subsidence caused via construction [10–12], and so engineers combined the pipe curtain structure with the PBA method to build shallowly buried subway stations.

Several metro stations have been successfully built in China using the above method, such as the Aotizhongxin station on Line 9, the Dongbeidamalu station on Line 10 of Shenyang Metro [13] and the Pinganli station on Line 19 of Beijing Metro. In the above cases, the surface subsidence resulting from the excavation of the pilot tunnel under the pipe curtain support accounted for about 50–60% of the overall subsidence, which shows that the construction of the pilot tunnel was a critical stage in the construction of the stations. Therefore, the study of the deformation response caused via the excavation of pilot tunnels under pipe curtain support is of great significance in predicting the strata deformation and controlling surface subsidence in the construction of stations.

There have been many studies on the deformation of strata and structures caused via construction using the pipe curtain method, but there is a lack of research on the deformation response caused via the excavation of pilot tunnels under pipe curtain support. Yang and Li [14] studied the surface subsidence pattern caused via the construction of the pipe curtain pre-construction method and established a surface subsidence prediction model based on the Peck formula. Shimada et al. [15] analyzed the limiting effect of the pipe curtain on the surrounding soil in conjunction with numerical simulations. Wang et al. [16]

explored the impact of flanged steel pipe jacking on the surface subsidence. Xie et al. [17,18] studied the surface subsidence pattern and soil pressure distribution caused via excavation under the action of the pipe curtain through model tests and established a theoretical model for the instability. Lu et al. [19] studied the pipe curtain deformation and surface subsidence patterns caused via large-section excavation under the novel pipe curtain structure support and derived the optimal construction parameters based on fuzzy mathematical theory. The research in the above literature focuses on two aspects: one is to study the impact of pipe jacking construction on surface subsidence and the other is to study the impact of the excavation of large sections on the deformation characteristics of the surface and the structure. The deformation response caused via the excavation of the pilot tunnel has not been studied in depth. Furthermore, in the above studies, the excavation direction is mostly parallel to the axis of the pipe curtain. However, the flexural stiffness of the pipe curtain structure under overlying loads is variable for different arrangements and therefore the deformation pattern caused via excavation is also different.

Given this, based on the Shenyang Metro Line 4 Shifu Road station, this paper conducts a study on the deformation response caused via the excavation of the transverse pilot tunnel (excavation direction perpendicular to the axis of the pipe curtain) under the support of the pipe curtain structure. Parameters such as excavation sequence, grouting width on both sides and temporary support strength of the transverse pilot tunnel were first investigated through numerical simulation to guide the design scheme. The influence on the deformation characteristics of the pipe curtain during actual construction resulting from the excavation of the transverse pilot tunnel was then investigated through on-site monitoring.

This paper describes a novel pipe curtain method for constructing subway stations. The method can realize the efficient utilization of underground space. The findings of the study can inform the further application of the method, and will provide new ideas for the construction of subway stations and other underground projects. It plays a good role in promoting the sustainable development of underground space.

2. Engineering Background

The dimensions of the Shifu Road station are 47.5 m (length) \times 26.5 m (width) \times 15.7 m (height), with an overburden of approximately 4.2 m. Figure 1 shows the cross-section. The station is located in a busy urban area with many high-rise buildings above, and so surface subsidence caused via construction needed to be strictly controlled. The PBA method currently in use could not be used because the thickness of the overburden on the station did not meet the requirements for the buckling arch. In addition, as the station is an interchange with the planned Shenyang Metro Line 7, the government requested that the construction period be shortened as much as possible. The existing pipe curtain methods, while providing good control of the surface subsidence, often require cutting adjacent steel pipes or adding bolts between pipes, which results in longer construction periods [20]. It was therefore decided to use the small pipe curtain–beam method for the construction of Shifu Road station.

In this method, the major steps of construction are illustrated in Figure 2 and were divided into four steps. This paper focuses on the effect on surface subsidence and pipe curtain deformation as a result of the excavation of the transverse pilot tunnel.

Step 1: The steel pipe was first jacked in to form the pipe curtain structure and then the Z1, Z2 and Z3 longitudinal pilot tunnels were excavated under the pipe curtain support. Subsequently, the bottom longitudinal beam, strip foundations and side piles were constructed in the longitudinal pilot tunnels.

Step 2: seven transverse pilot tunnels were excavated in the Z3 pilot tunnel and beams and intermediate columns were constructed in the transverse pilot tunnels.

Step 3: excavating the negative layer of soil and constructing the top slab, upper side walls and middle slab.

Step 4: excavating the negative two layers of soil and constructing the top slab, lower side walls and bottom slab.

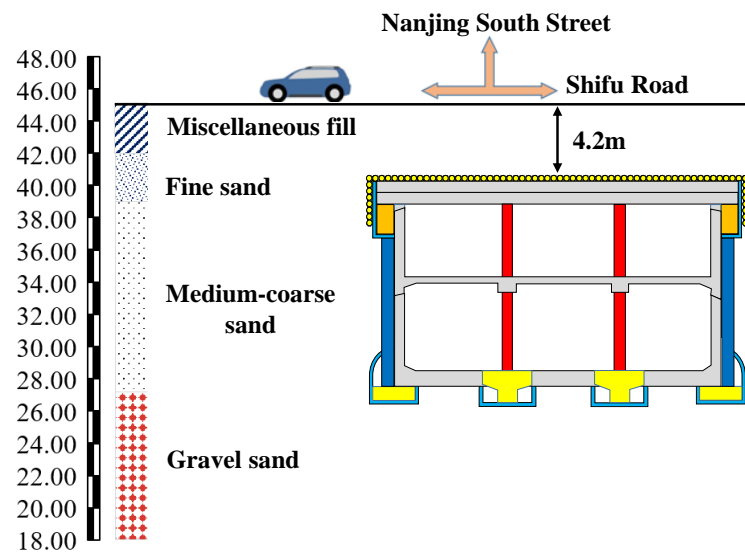


Figure 1. The section of the station.

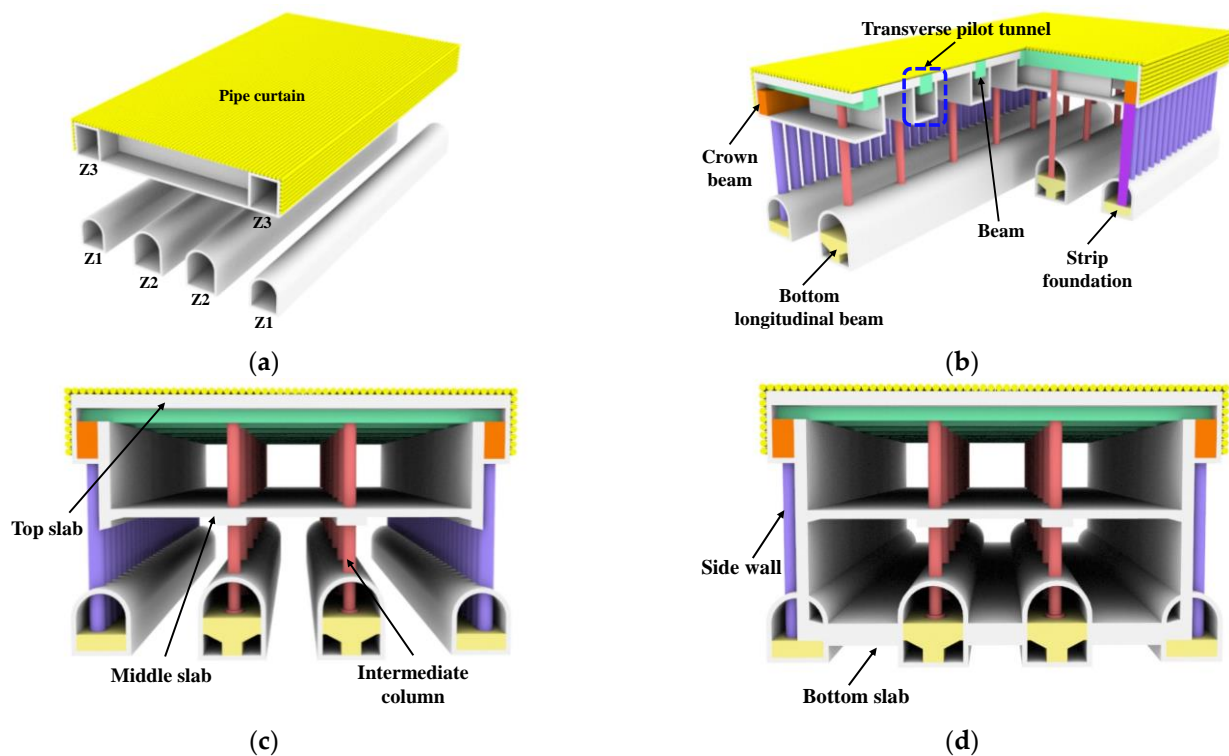


Figure 2. Main construction process: (a) Step 1. (b) Step 2. (c) Step 3. (d) Step 4.

In this method, seven beams were erected below the pipe curtain to form a pipe curtain–beam support system. Figure 3 is a schematic diagram of the transverse pilot tunnel. The steel pipes have a diameter of 402 mm, spacing of 450 mm and a wall thickness of 16 mm. The beams are located in the transverse pilot tunnel, which has a cross-sectional dimension of approximately $3.8 \text{ m} \times 4.2 \text{ m}$ and a center distance of approximately 7.5 m. As this was the first application of the method, the construction parameters of the transverse pilot tunnel needed to be investigated to determine a reasonable construction plan. H denotes the number of the pilot tunnel.

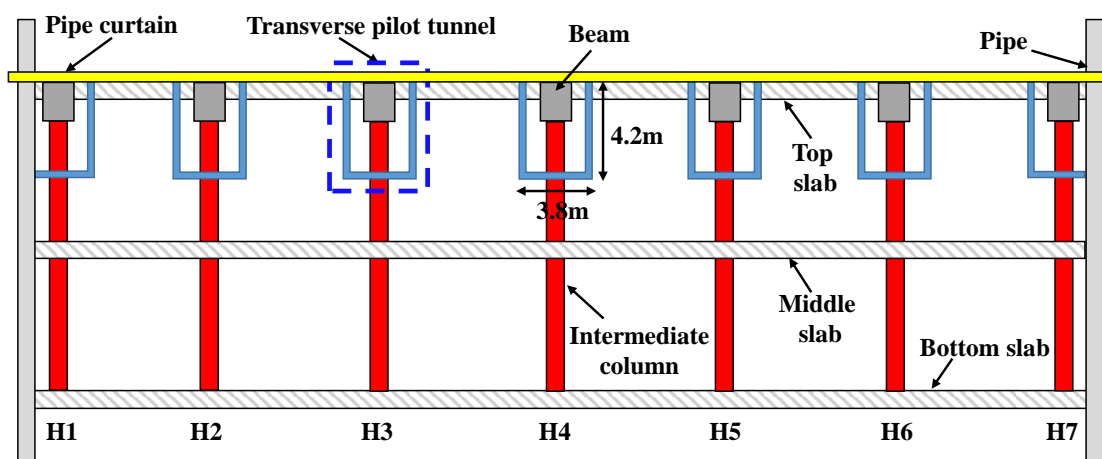


Figure 3. Schematic diagram of the transverse pilot tunnel.

3. Analysis of Key Parameters of Transverse Pilot Tunnel

To avoid the “group tunnels effect”, it is necessary to investigate the construction sequence of the transverse pilot tunnel. In addition, the grouting reinforcement before excavation and initial support after excavation of the pilot tunnel can reduce the surface subsidence and pipe curtain deformation caused via construction. Therefore, the width of the grouting reinforcement and the strength of the initial support should be considered. In this section, the Midas GTS NX, v. 2017 R2, software was used to simulate the construction process of the transverse pilot tunnel and to study the effects of changes in parameters, such as the construction sequence of the pilot tunnel, the grouting width on both sides of the pilot tunnel and the strength of the initial support on the strata and structure.

3.1. Numerical Model and Parameters

To avoid the impact of boundary conditions on the calculation results, the size of the model was set as $150\text{ m} \times 47.5\text{ m} \times 50\text{ m}$ (Figure 4). The bottom of the model was fixed, the normal displacement was constrained around it and the top was a free surface. A ground overload of 20 kPa was applied above the model [4,21]. All strata were simplified to a uniform distribution [22], with thicknesses of 3.0 m, 11.2 m, 24.5 m and 11.3 m from top to bottom. An elastic constitutive was applied to the pipe curtain. A solid element was used to simulate the soil and a beam element was used to simulate the pipe curtain. There was a disjunction between the primary lining and the pipe curtain on the solid element. The element killing method was used to realize the excavation of the pilot tunnel. The elastic modulus of the pipe curtain was calculated using the principle of equivalent bending stiffness [20]. Since the flexural stiffness of the interlock was far less even than the flexural stiffness of the steel tube in the longitudinal direction [18], the interlock was not considered in this paper. The grouting of the sides of the transverse pilot tunnel in the model was achieved using the changing properties function of the software. Dewatering will be applied before construction, and so the effect of groundwater was not considered. The model consists of units and a grand total of 232,275 nodes. The major stratigraphic and structural parameters are illustrated in Table 1.

The numerical simulation was simplified into three main steps: pipe curtain jacking, excavation of the longitudinal pilot tunnel and excavation of the transverse pilot tunnel. In the process of subway station construction, the surface subsidence directly reflects the safety of the subway station, and so the change in surface subsidence with excavation is often something to consider. Pipe curtain deformation is a key factor affecting surface subsidence. Therefore, in this paper, surface subsidence and pipe curtain deformation have been analyzed mainly in the numerical simulation.

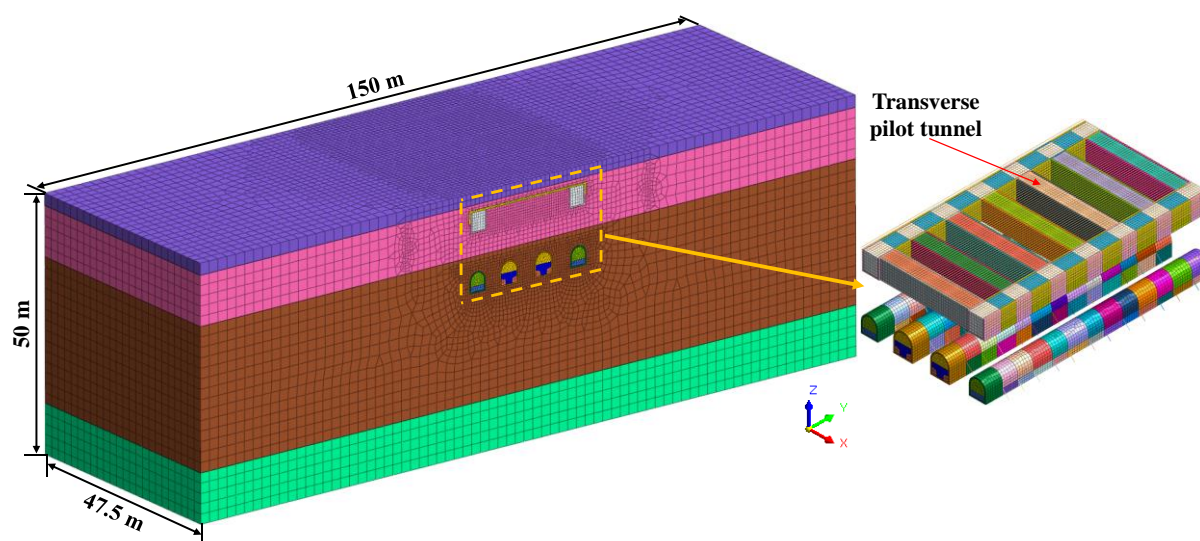


Figure 4. Numerical calculation model.

Table 1. Material properties.

Stratum/Structure	Density ($\text{kg}\cdot\text{m}^{-3}$)	Young's Modulus (MPa)	Poisson's Ratio	Cohesion (kPa)	Internal Friction Angle ($^{\circ}$)
Miscellaneous fill	2000	15.0	0.28	4.0	26.0
Pipe curtain	3000		0.25	/	/
Medium-coarse sand	1930	15.5	0.28	2.0	35.0
Fine sand	1890	9.5	0.30	3.0	22.7
Gravel sand	1960	26.6	0.29	2.0	36.7
Primary lining	2400		0.20	/	/

3.2. Analysis of the Simulation Results

3.2.1. Excavation Sequence

To investigate the impact of the excavation sequence on surface subsidence and pipe curtain deformation, three excavation sequences were selected. Moreover, to obtain an obvious change law, both sides of the transverse pilot tunnel were not reinforced by grouting. The excavation sequence is as follows:

Case 1: H2 and H4 and H6 → H1 and H3 → H5 and H7

Case 2: H3 and H4 and H5 → H2 and H6 → H1 and H7

Case 3: H1 and H3 → H5 and H7 → H2 and H4 and H6

Figure 5 shows the surface subsidence curve of the longitudinal section caused via the excavation of different transverse pilot tunnels under the same case. It can be seen from the figure that the change in subsidence is mainly affected by the construction of the transverse pilot tunnel directly below. When Case 1 is adopted, the subsidence curve presents a “wave” shape after the excavation of the first step, and the difference between the crest and trough is large. After the excavation of the second step, the left side of the subsidence curve increases significantly; after the excavation of the third step, the subsidence curve presents a “wave” shape, and the curve is relatively moderate in general. When Case 2 is adopted, the subsidence curves after the three excavation steps are similar in shape. When Case 3 is adopted, after the excavation of the first step, the subsidence curve presents a trend of first increasing and then decreasing. After the excavation of the second step, the change trend of the subsidence curve is consistent with the construction of the double-line tunnel; after the excavation of the third step, the subsidence curve presents a “wave” shape, consistent with the other two cases.

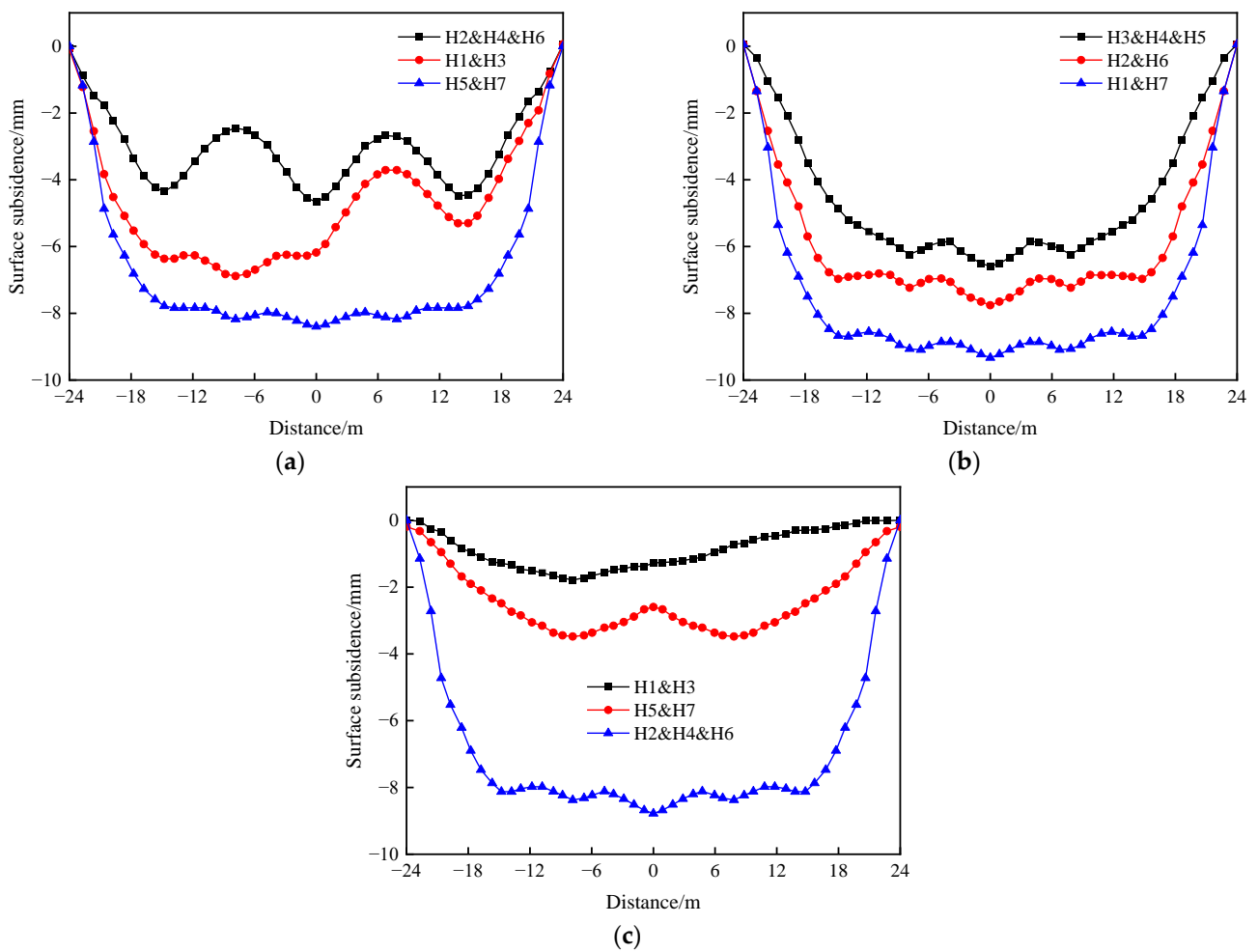


Figure 5. Deformation curves at different steps of transverse pilot tunnel construction: (a) Case 1. (b) Case 2. (c) Case 3.

Figure 6 shows the stacking diagram of surface subsidence for different cases. For Case 1 and Case 3, the surface subsidence resulting from the excavation of the H2, H4 and H6 pilot tunnels accounted for 55.9% and 60% of the overall subsidence, respectively. For Case 2, the surface subsidence resulting from the excavation of the H3, H4 and H5 pilot tunnels accounted for 70.9% of the total subsidence. It can be seen that the excavation of the central pilot tunnels is the key stage of construction, and the support of the central pilot tunnels should be strengthened during construction on time.

The surface subsidence in the transverse section and longitudinal section under different excavation sequences is indicated in Figure 7. From the figure, the surface subsidence curve in the transverse section has a “groove” shape, and the surface subsidence curve in the longitudinal section has a “wave” shape. In terms of final surface subsidence, Case 2 (9.29 mm) > Case 3 (8.74 mm) > Case 1 (8.29 mm). For “Case 3 > Case 1”, it can be concluded that the surface subsidence generated via the excavation sequence of “excavating both side pilot tunnels first and then excavating middle pilot tunnels” is greater than that of “excavating middle pilot tunnels first and then both side pilot tunnels”. For “Case 2 > Case 1”, it can be concluded that the surface subsidence resulting from the excavation sequence of “simultaneously excavating the three middle pilot tunnels” is greater than that of “excavating the three middle pilot tunnels at intervals”.

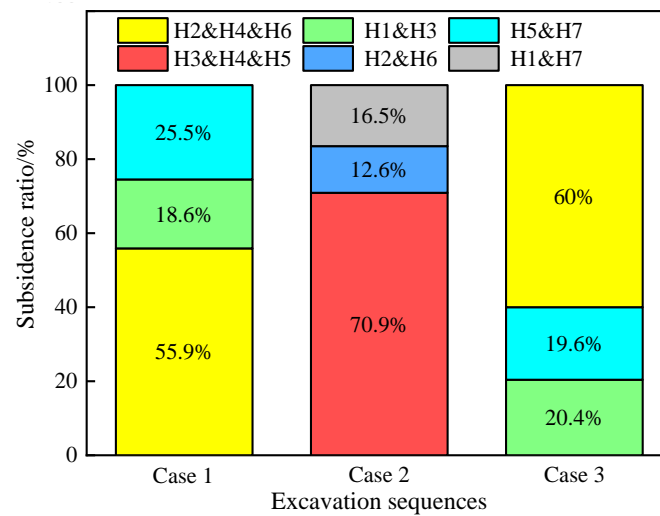


Figure 6. Histogram of surface subsidence in pilot tunnel excavation.

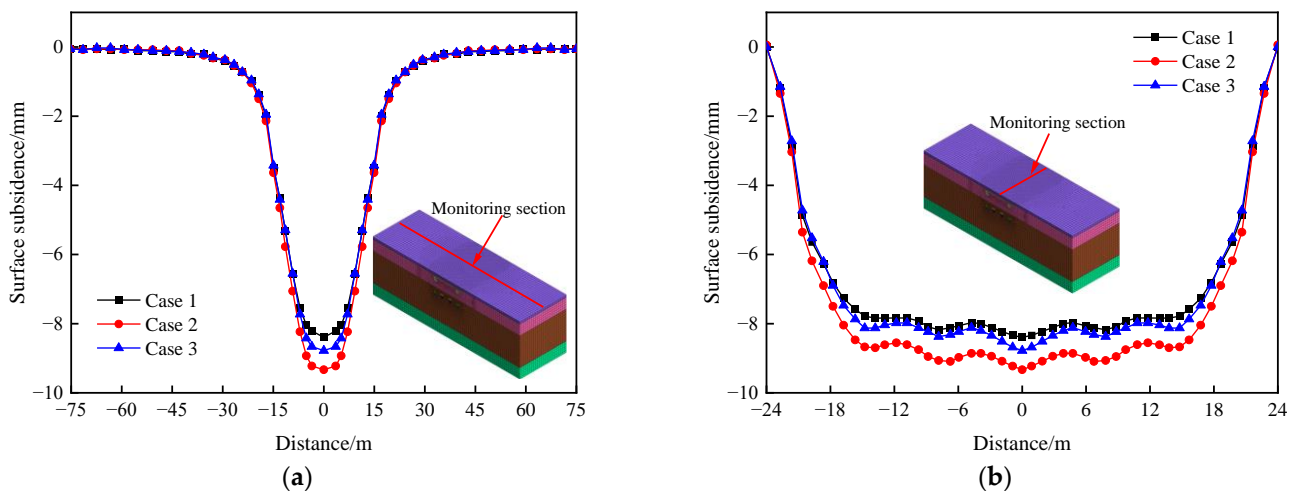


Figure 7. Surface subsidence under different excavation sequences: (a) Transverse surface subsidence. (b) Longitudinal surface subsidence.

Figure 8 shows the deformation and bending moment of the pipe curtain under different excavation sequences. From the figure, it can be seen that for Cases 1, 2 and 3, the maximum values of pipe curtain deformation after excavation are 9.39 mm, 10.33 mm and 9.78 mm, respectively, and the maximum values of the bending moment are 75.22 kN·m, 88.57 kN·m and 83.26 kN·m, respectively. In conclusion, the surface subsidence, pipe curtain deformation and bending moment of the pipe curtain resulting from the excavation of Case 1 are the lowest. In addition, after the excavation of the transverse pilot tunnel, the variation trend of pipe curtain deformation is consistent with the surface subsidence of the longitudinal section, and the pipe curtain deformation is always greater than the surface subsidence. It can be seen that the surface subsidence resulting from the excavation of the transverse pilot tunnel is mainly affected by the pipe curtain deformation. Therefore, the pipe curtain deformation is mainly analyzed in the following research.

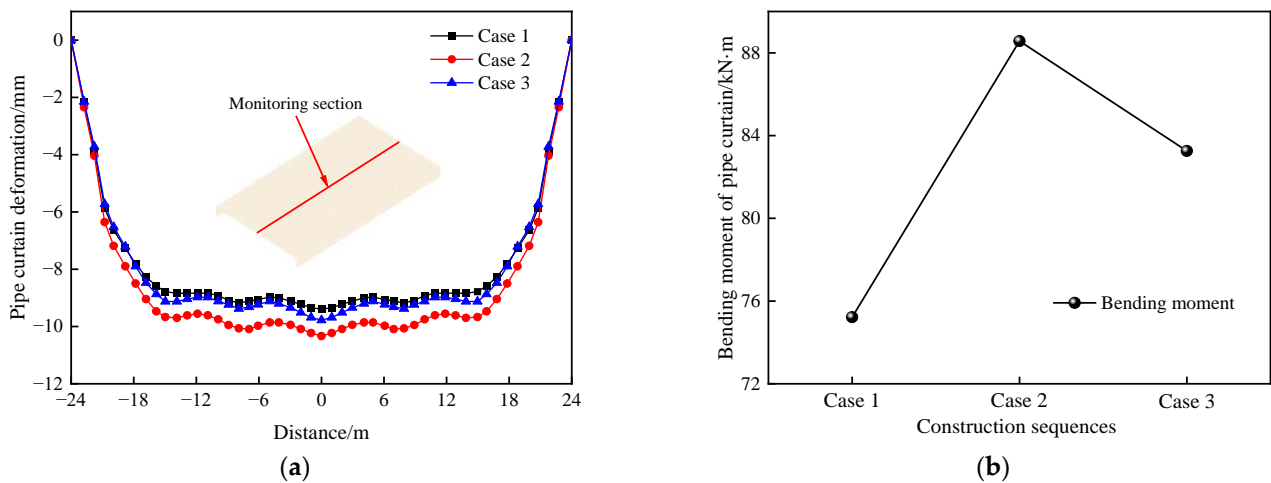


Figure 8. Deformation and bending moment of pipe curtain under different excavation sequences: (a) Pipe curtain deformation. (b) Bending moment of pipe curtain.

3.2.2. Width of the Grouting Reinforcement

A reasonable grouting width can effectively control the pipe curtain deformation. According to the above research results, it is safer to use Case 1 to excavate the transverse pilot tunnel. The excavation of the H2, H4 and H6 pilot tunnels is the key stage of construction. Therefore, both sides of the H2, H4 and H6 pilot tunnels were selected for grouting reinforcement. The grouting widths were selected as 0 m (without grouting), 1 m, 1.5 m and 2.0 m. Figure 9 shows the maximum pipe curtain deformation under different grouting widths. As can be seen from the figure, the pipe curtain deformation gradually decreases with the increase in grouting width, and the grouting width and the maximum value of pipe curtain deformation conform to a linear relationship. Compared with the grouting width of 0 m, when the grouting width is 1 m, 1.5 m and 2.0 m, the maximum value of the pipe curtain deformation decreases by 13.74%, 27.47% and 30.56%, respectively, and the latter two grouting widths have similar control effects on pipe curtain deformation. In conclusion, it is reasonable to choose a 1.5 m grouting width.

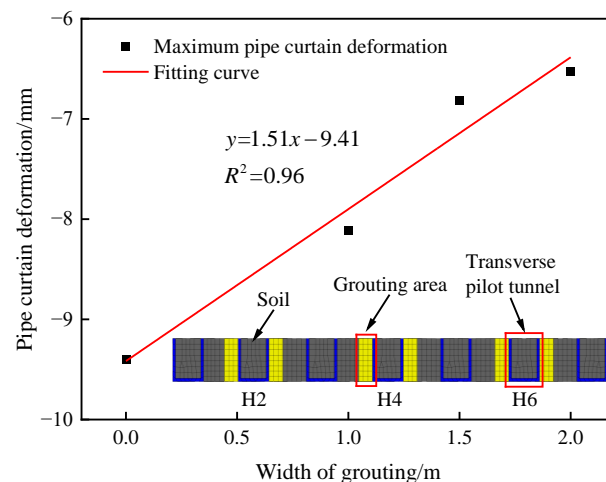


Figure 9. Pipe curtain deformation under different widths of grouting.

3.2.3. Strength of the Initial Support

During the excavation of the transverse pilot tunnel, an overly high initial support strength may easily result in wasted material, while an overly low initial support strength may result in greater pipe curtain deformation. Therefore, in this section, the effect of the initial support strength on the pipe curtain deformation is investigated. In the design

scheme of the relying project, steel arches and C25 concrete are used as the initial support. To facilitate the numerical modeling, the steel arch and concrete are simplified to a whole according to the principle of stiffness equivalence and are simulated using solid units. Different support strengths are indicated by varying the elastic modulus of the solid units. The support strengths were chosen to be 0.5, 1, 1.5 and 2 times the design scheme. The maximum values of pipe curtain deformation for different support strengths are shown in Figure 10. From the figure, the pipe curtain deformation gradually decreases as the strength of the support increases. Compared to the design scheme, the pipe curtain deformation increases by 40.04% when the support strength is 0.5 times that of the design scheme. For 1.5 times and 2 times the design scheme, the pipe curtain deformation is reduced by 19.16% and 22.89%, respectively, within 4% of each other. It can be seen that when the support strength is 1.5 times the design scheme, the initial support has already played a full role in controlling the deformation, and a further increase in the support strength cannot significantly reduce the pipe curtain deformation. Compared with the method of increasing the grouting width to control the pipe curtain deformation, the effect of increasing the support strength to control the pipe curtain deformation is not obvious. Therefore, in the actual construction, the grouting reinforcement on both sides of the transverse pilot tunnel was chosen to control the pipe curtain deformation, and the initial support strength was set according to the original design scheme.

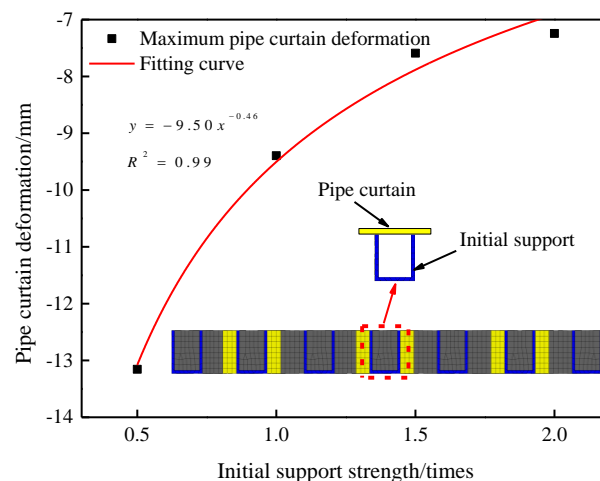


Figure 10. Pipe curtain deformation under different support strengths.

4. Analysis of Field Monitoring Data

The deformation characteristics of the pipe curtain structure are an important reference for the safe construction of the station, and monitoring points are arranged to study the deformation and strain of the pipe curtain during the construction of the transverse pilot tunnel. In addition, the steel arches need to be broken before excavating the transverse pilot tunnel. For reducing perturbation resulting from breaking the steel arch, a “door” type temporary support will be set up before the steel arch is broken. When the steel arch is broken, the temporary support becomes the main load-bearing structure, carrying the overlying loads. Therefore, monitoring points are placed on the temporary support to analyze the strain pattern of the temporary support during the breakage of the steel arch.

Figure 11 shows the arrangement of monitoring points for deformation and strain of the pipe curtain. The monitoring points of the pipe curtain deformation were arranged inside the steel pipe, measured using an automatic hydrostatic level system [23], and a total of four monitoring sections (P1–P4) were arranged, whereby each section had five monitoring points and the monitoring point spacing was about 8 m. The pipe curtain strain was measured using strain gauges. When arranging monitoring points for the pipe curtain strain, owing to the constraints of the on-site conditions, only two sets of monitoring points were arranged. One group was installed above the middle of the H7 pilot tunnel to measure

the pipe curtain strain during the excavation of the transverse pilot tunnel, and the other group was installed at the entrance of the H5 pilot tunnel to measure the pipe curtain strain during the breaking of the steel arch. Figure 12 shows the arrangement of the monitoring points of the temporary support strains, with a total of two strain gauges arranged to measure the strains in the horizontal and vertical temporary supports, respectively.

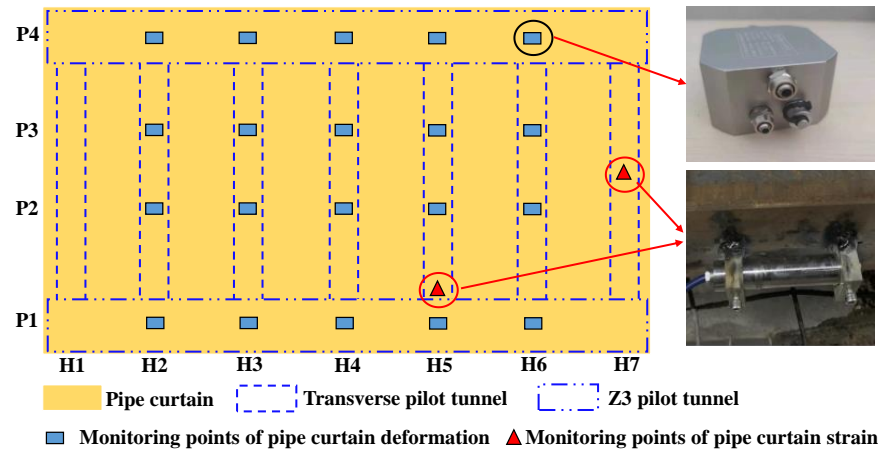


Figure 11. Arrangement of monitoring points of pipe curtain.

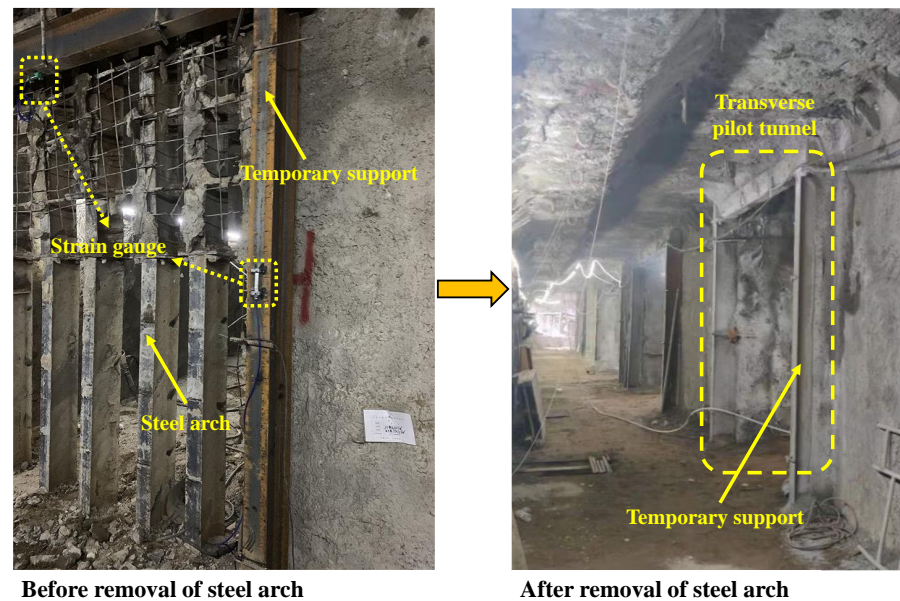


Figure 12. Arrangement of monitoring points of temporary support.

The pipe curtain deformation in section P3 and section P4 is indicated in Figure 13. From Figure 13a, pipe curtain deformation at P3-1, P3-3 and P3-5 shows the same trend over time, first increasing sharply and then gradually stabilizing. The variation in pipe curtain deformation at P3-2 and P3-4 is similar, which increases slowly at first, then increases sharply and then becomes stable gradually. And, the pipe curtain deformation at P3-1, P3-3 and P3-5 is significantly greater than that at P3-2 and P3-4. This is a result of the construction sequence of the transverse pilot tunnel. After the excavation of the transverse pilot tunnel, the maximum pipe curtain deformation on section P3 is located at P3-3, which is about 8.3 mm. From Figure 13b, the variation law of pipe curtain deformation at each monitoring point in section P4 with time is generally the same as that in section P3. However, the pipe curtain deformation of these monitoring points is in a state of fluctuation, which is because the monitoring point on section P4 is located above the Z3 pilot tunnel, and workers and transport vehicles enter and exit through the Z3 pilot tunnel. The maximum pipe curtain

deformation on section P4 is no more than 4 mm, indicating that the excavation of the transverse pilot tunnel has a greater impact on pipe curtain deformation above the middle of the station.

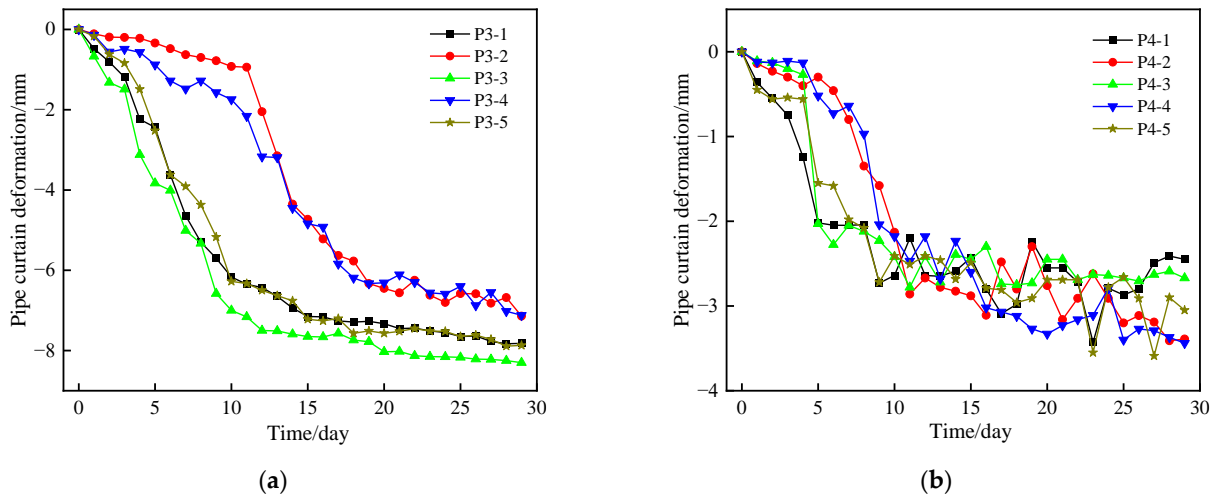


Figure 13. Pipe curtain deformation: (a) Section P3. (b) Section P4.

Figure 14 shows the pipe curtain strain during the excavation of the transverse pilot tunnel. From Figure 14a, the pipe curtain strain in the mid-span of the H7 pilot tunnel gradually increases and then stabilizes as the excavation face continues to advance. When the distance between the excavation face and the monitoring point is within 1 m, the pipe curtain strain increases at the fastest rate, which is about $150 \mu\epsilon/m$. When the distance between the excavation face and the monitoring point is 2 m, the pipe curtain strain reaches the maximum, and then the strain tends to stabilize. From Figure 14b, the pipe curtain strain at the entrance of the H5 pilot tunnel is divided into three main stages during the steel arch breaking process: The first is the slow growth stage, in which the concrete lining at the entrance of the pilot tunnel is broken. The second is the rapid development stage, where the steel arch is broken down and the pipe curtain strain increases sharply with a rate of change of approximately $35 \mu\epsilon/h$. The third is the stabilization stage, whereby the steel arch is completely broken down and the pipe curtain strain stabilizes with a final strain value of approximately $95 \mu\epsilon$.

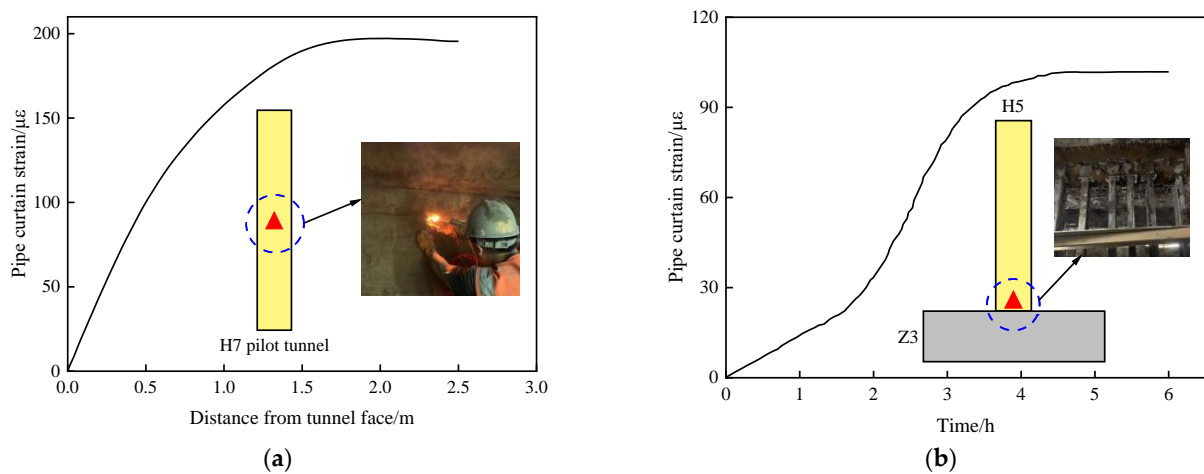


Figure 14. Pipe curtain strain: (a) Mid-span of H7 pilot tunnel. (b) Entrance of H5 pilot tunnel.

Figure 15 shows the strain curve for the temporary support during the removal of the steel arch. It can be seen that the trends in the strain curves for the horizontal and vertical temporary supports are similar overall, and could be classified into three stages:

The first is the slow growth stage, in which the concrete lining of the longitudinal pilot tunnel is broken, and when the lining is broken, the strain values of horizontal and vertical temporary support are $24 \mu\epsilon$ and $18 \mu\epsilon$, respectively. The second is the rapid development stage, whereby during which the steel arches are removed and the overlying loads are carried by the temporary supports, leading to a rapid increase in strain values, reaching $101 \mu\epsilon$ and $79 \mu\epsilon$ for the horizontal and vertical temporary supports, respectively. The third is the stabilization stage, where the steel arch is completely removed and the strain values stabilize, with final strain values of $107 \mu\epsilon$ and $82 \mu\epsilon$ for the horizontal and vertical temporary supports, respectively. Throughout the breaking process, the strain values for the horizontal temporary support are always greater than the vertical strain values. This is because the horizontal temporary support is located directly below the pipe curtain, and when the steel arch is removed, the overlying load acts on the horizontal temporary support first, resulting in a higher strain value.

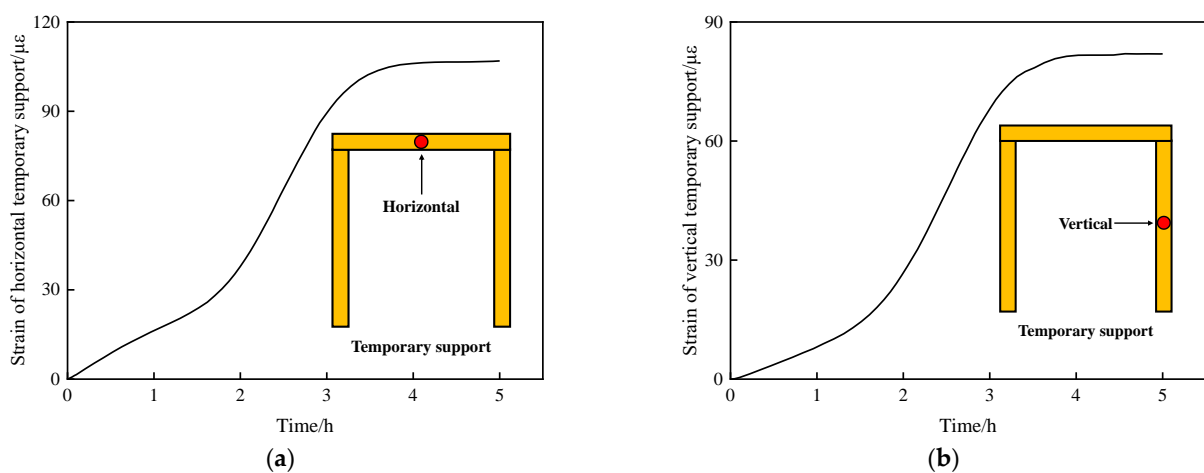


Figure 15. Strain of temporary support: (a) Horizontal. (b) Vertical.

Figure 16 shows a comparison at P3-3 and P4-3. During the excavation of the transverse pilot tunnel, the simulation results of the pipe curtain deformation at the two monitoring points are close to the monitoring results and the trend is consistent. At the end of the excavation, the monitoring values of pipe curtain deformation at P3-3 and P4-3 are 8.3 mm and 2.67 mm, and the simulation values are 8.51 mm and 2.81 mm, with an error of 2.46% and 4.98%, respectively, with both within 5%. It can be seen that the simulation results are in good agreement with the monitoring results, confirming the reasonableness of the numerical simulation.

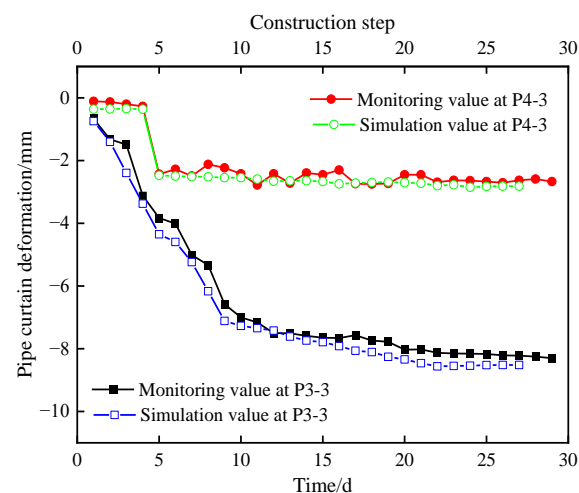


Figure 16. Comparison of monitoring values and simulation values.

5. Conclusions

In this paper, the surface subsidence and pipe curtain deformation resulting from the excavation of the transverse pilot tunnel were investigated through numerical simulation and field monitoring, and the following conclusions were obtained:

- (1) The change in subsidence is mainly affected by the construction of the transverse pilot tunnel directly below. The excavation of the middle pilot tunnel is the key stage of the construction.
- (2) When the excavation sequence of the pilot tunnel is H2 and H4 and H6 → H1 and H3 → H5 and H7, the surface subsidence caused via excavation is the smallest, and the construction is safer.
- (3) The maximum pipe curtain deformation and the grouting width follow a linear relationship, and the grouting width of 1.5 m is more reasonable.
- (4) Compared with increasing the grouting width, the effect of increasing the initial support strength of the pilot tunnel to control the pipe curtain deformation is not obvious.
- (5) The pipe curtain strain in the mid-span of the transverse pilot tunnel gradually increases and then stabilizes. The pipe curtain strain at the entrance of the pilot tunnel is mainly divided into three stages: “slow growth”, “rapid development” and “stabilization” during the breaking of the steel arch.

Author Contributions: Q.B.: conceptualization, methodology, writing—original draft. W.Z.: supervision, methodology, writing—review and editing. Y.S.: investigation. X.W.: writing—review and editing. All authors have read and agreed to the published version of the manuscript.

Funding: The research described in this paper was supported by the National Natural Science Foundation of China (51878127).

Conflicts of Interest: The authors declare no conflict of interest.

References

1. Chen, Y.; Tan, L.; Xiao, N.; Liu, K.; Jia, P.; Zhang, W. The hydro-mechanical characteristics and micro-structure of loess enhanced by microbially induced carbonate precipitation. *Geomech. Energy Environ.* **2023**, *34*, 100469.
2. Han, J.Y.; Wang, J.; Jia, D.F.; Yan, F.S.; Zhao, Y.; Bai, X.Y.; Yan, N.; Yang, G.; Liu, D. Construction technologies and mechanical effects of the pipe-jacking crossing anchor-cable group in soft stratum. *Front. Earth Sci.* **2023**, *10*, 1019801. [[CrossRef](#)]
3. Wang, Z.Z.; Chen, C. Fuzzy comprehensive Bayesian network-based safety risk assessment for metro construction projects. *Tunn. Undergr. Space Technol.* **2017**, *70*, 330–342. [[CrossRef](#)]
4. Han, J.Y.; Wang, J.; Cheng, C.; Zhang, C.Z.; Liang, E.B.; Wang, Z.K.; Song, J.J.; Leem, J.S. Mechanical response and parametric analysis of a deep excavation structure overlying an existing subway station: A case study of the Beijing subway station expansion. *Front. Earth Sci.* **2023**, *10*, 1079837. [[CrossRef](#)]
5. Wang, Q.; Geng, P.; Guo, X.Y.; Wang, X.Q.; Li, P.S.; Zhao, B.B. Case study on the seismic response of a subway station combined with a flyover. *Undergr. Space* **2021**, *6*, 665–677. [[CrossRef](#)]
6. Liu, X.R.; Liu, Y.G.; Yang, Z.P.; He, C.M. Numerical analysis on the mechanical performance of supporting structures and ground settlement characteristics in construction process of subway station built by Pile-Beam-Arch method. *KSCE J. Civ. Eng.* **2017**, *21*, 1690–1705. [[CrossRef](#)]
7. Yu, L.; Zhang, D.L.; Fang, Q.; Cao, L.Q.; Xu, T.; Li, Q.Q. Surface settlement of subway station construction using pile-beam-arch approach. *Tunn. Undergr. Space Technol.* **2019**, *90*, 340–356.
8. Xu, X.; Li, Z.; Fang, Q.; Zheng, H. Challenges and countermeasures for using pile-beam-arch approach to enlarge large-diameter shield tunnel to subway station. *Tunn. Undergr. Space Technol.* **2020**, *98*, 103326. [[CrossRef](#)]
9. Guo, X.Y.; Wang, Z.Z.; Geng, P.; Chen, C.J.; Zhang, J. Ground surface settlement response to subway station construction activities using pile-beam-arch method. *Tunn. Undergr. Space Technol.* **2021**, *108*, 103729. [[CrossRef](#)]
10. Kang, Y.S.; Liu, Q.S.; Cheng, Y.; Liu, X.Y. Combined freeze-sealing and New Tubular Roof construction methods for seaside urban tunnel in soft ground. *Tunn. Undergr. Space Technol.* **2016**, *58*, 1–10. [[CrossRef](#)]
11. Liu, J.G.; Ma, B.S.; Cheng, Y. Design of the Gongbei tunnel using a very large cross-section pipe-roof and soil freezing method. *Tunn. Undergr. Space Technol.* **2018**, *72*, 28–40. [[CrossRef](#)]
12. Yang, S.S.; Wang, M.; Du, J.N.; Guo, Y.; Geng, Y.; Li, T. Research of jacking force of densely arranged pipe jacks process in pipe-roof pre-construction method. *Tunn. Undergr. Space Technol.* **2020**, *97*, 103277. [[CrossRef](#)]
13. Jia, P.J.; Nie, Y.T.; Shi, P.X.; Jiang, X.; Lu, B.; Zhao, W. Flexural performance of a novel pipe-roof structure and optimization of key parameters. *J. Constr. Steel Res.* **2022**, *199*, 107594. [[CrossRef](#)]

14. Yang, X.; Li, Y.S. Research of surface settlement for a single arch long-span subway station using the Pipe-roof Pre-construction Method. *Tunn. Undergr. Space Technol.* **2018**, *72*, 210–217. [[CrossRef](#)]
15. Shimada, H.; Khazaei, S.; Matsui, K. Small diameter tunnel excavation method using slurry pipe-jacking. *Geotech. Geol. Eng.* **2004**, *22*, 161–186. [[CrossRef](#)]
16. Wang, Z.G.; Zhao, W.; Wang, H.; Chen, Y.; Bai, Q.; Li, S.G. Analysis of the influence of geometrical parameters of circular steel pipe with flange plate on the jacking force. *Undergr. Space.* **2022**, *7*, 324–336. [[CrossRef](#)]
17. Xie, X.Y.; Zhao, M.R.; Shahrour, I. Face stability model for rectangular large excavations reinforced by pipe roofing. *Tunn. Undergr. Space Technol.* **2019**, *94*, 103132. [[CrossRef](#)]
18. Xie, X.Y.; Zhao, M.R.; Shahrour, I. Experimental study of the behavior of rectangular excavations supported by a pipe roof. *Appl. Sci.* **2019**, *9*, 2082. [[CrossRef](#)]
19. Lu, B.; Dong, J.C.; Zhao, W.; Du, X.; Cheng, C.; Bai, Q.; Wang, Z.G.; Zhao, M.C.; Han, J.Y. Novel pipe-roof method for a super shallow buried and large-span metro underground station. *Undergr. Space* **2022**, *7*, 134–150. [[CrossRef](#)]
20. Bai, Q.; Zhao, W.; Cao, W.X.; Jia, P.J.; Cheng, C.; Lu, B. Test and numerical simulation of excavation of subway stations using the small pipe-roof-beam method. *Int. J. Geomech.* **2023**, *23*, 04023018. [[CrossRef](#)]
21. Jia, P.J.; Zhao, W.; Chen, Y.; Li, S.G.; Han, J.Y.; Dong, J.C. A case study on the application of the steel tube slab structure in construction of a subway station. *Appl. Sci.* **2018**, *8*, 1437. [[CrossRef](#)]
22. Galliková, Z.; ur Rehman, Z. Appraisal of the hypoplastic model for the numerical prediction of high-rise building settlement in Neogene clay based on real-scale monitoring data. *J. Build. Eng.* **2022**, *50*, 104152. [[CrossRef](#)]
23. Zhang, C.P.; Zhang, X.; Fang, Q. Behaviors of existing twin subway tunnels due to new subway station excavation below in close vicinity. *Tunn. Undergr. Space Technol.* **2018**, *81*, 121–128. [[CrossRef](#)]

Disclaimer/Publisher’s Note: The statements, opinions and data contained in all publications are solely those of the individual author(s) and contributor(s) and not of MDPI and/or the editor(s). MDPI and/or the editor(s) disclaim responsibility for any injury to people or property resulting from any ideas, methods, instructions or products referred to in the content.